Available online at www.sciencedirect.com

SciVerse ScienceDirect

Ceramics International 38 (2012) 1331–1339

CERAMICS INTERNATIONAL

www.elsevier.com/locate/ceramint

Effect of sol composition on dielectric and ferroelectric properties of PZT composite films

Anupama Sachdeva [a,b], R.P. Tandon [a,*]

[a] Department of Physics and Astrophysics, University of Delhi, Delhi 110007, India
[b] Keshav Mahavidyalaya, University of Delhi, Delhi 110034, India

Received 25 June 2011; received in revised form 2 September 2011; accepted 3 September 2011
Available online 10 September 2011

Abstract

Crack free calcium modified PZT composite films have been synthesized using modified sol–gel process by depositing the slurries prepared by mixing powder of composition $PbZr_{0.52}Ti_{0.48}O_3$ and sol of composition $Pb_{(1-x)}Ca_xZr_{0.52}Ti_{0.48}O_3$ (where $x = 0$, 0.06, 0.1) on Pt(1 1 1)/Ti/SiO_2/Si substrate. The infilteration process has also been employed which resulted in dense microstructure of the films. Thickness of the films as measured by SEM of cross section of the films was more than 25 μm. The XRD patterns of the resultant films consisted of pure perovskite phase and no peak related to either pyrochlore phase or Pt substrate was observed. The room temperature dielectric constant and loss were compared. The temperature dependence of dielectric constant revealed that T_C of all the films was same, i.e., 351 °C, in spite of different compositions of the sol used. Well saturated PE-loops of the films show that the films were ferroelectric in nature.

Keywords: A. Sol–gel process, D. PZT; D. Perovskite; Infilteration process

1. Introduction

Thick PZT films are of great interest in actuation of active structures in MEMS [1–4]. Many applications use their sensor and actuation capabilities in various fields, e.g., medical, military, telecommunication, etc. The ferroelectric and piezoelectric properties of such films in the thickness range 5–100 μm make them suitable for integrated actuation applications. Thick film technology fills the technological gap between thin films and bulk ceramics because conventional thin film deposition processes can produce films with smaller thickness (a few microns) and bulk materials are hard to be manufactured with a thickness less than 100 μm. So, PZT ferroelectric thick films possess merits of both bulk materials and thin films. The density of the film also plays an important role in overall performance of the device. Therefore, preparing crack-free and dense thick films is of great significance. Recently, the tremendous growth of research on fabrication of PZT films has resulted in the development of many sophisticated PZT film synthesis techniques. Among these methods, sol–gel [5–8] is the most popular and widespread technique for its attractive advantages of simple set-up, low cost, low temperature processing conditions and good control over stoichiometry, hence excellent film properties. But the conventional sol–gel method suffers from serious drawbacks of cracking of films, hence considerable degradation of the properties and also low critical thickness [5,9,10]. Screen printing is one of the most commonly used processes for fabricating thick films with thickness larger than 10 μm. However, the films prepared by screen printing method have low density and require higher annealing temperatures (>800 °C). This high temperature processing results in damage of platinized silicon bottom electrode [11–13]. Therefore, modified sol–gel technique has been developed by Barrow et al. [14] in which annealed PZT powder is dispersed in sol–gel matrix to obtain paint like slurry which is when deposited on a substrate either by screen printing or by spin coating process results into thick films of thickness much greater than 1 μm. The resulting thick films are called 0–3 ceramic/ceramic composite films because the sol–gel matrix is connected in all the three directions and PZT powder is not connected in any direction. The main advantages of modified sol–gel method are:

* Corresponding author. Tel.: +91 11 27667725; fax: +91 11 27667061.
E-mail address: ram_tandon@hotmail.com (R.P. Tandon).

0272-8842/$36.00
doi:10.1016/j.ceramint.2011.09.009

1. The film forms strongly bonded network, with a sol–gel film firmly bonded between ceramic particles, making it less likely that the film will crack during processing.
2. Due to the presence of significant amount of ceramic powder, the percentage of sol–gel in the film is decreased and less shrinkage occurs when the film is processed.
3. Comparatively thicker films can be obtained.
4. Properties are comparable to bulk material.
5. We are dealing with a two-phase system (sol and powder) and therefore have greater opportunity to tailor the properties of the final films because of many permutations and combinations possible with the two phases. Some of these may be:
   - Altering powder to sol ratio.
   - Altering quality/composition of the powder.
   - Using different sizes of the powder.
   - Using different compositions of the sol keeping the composition of the powder fixed, etc.

So, in order to use the films for specific applications, it is important to understand how the above factors influence the properties of the final films.

Nevertheless, there is one major drawback of the films prepared from modified sol–gel process that the films are highly porous. Therefore, to obtain dense thick films is still a challenging job. In the present work, the infiltration process has also been employed to reduce the porosity [15–18] wherein after the deposition of the slurry on the substrate, PZT precursor solution is deposited on the composite film to infiltrate and fill-up the pores.

2. Experimental

2.1. Sol and slurry preparation

Calcium modified PZT precursor solutions with composition $Pb_xCa_{1-x}(Zr_{0.52}Ti_{0.48})O_3$ ($x = 0$, 0.06, 0.1) were prepared from lead acetate trihydrate ($Pb(CH_3COO)_2{\cdot}3H_2O$; >99%, Alfa Aesar), calcium acetate hydrate ($Ca(CH_3COO)_2{\cdot}H_2O$; 99%, Sigma Aldrich), zirconium propoxide ($Zr(OC_3H_7)_4$, 70 wt% in propanol; 99%, Aldrich) and titanium propoxide ($Ti(OC_3H_7)_4$; 98%, Aldrich). Glacial acetic acid and 2-methoxyethanol have been used as chelating agent and solvent respectively. The detail of sol preparation process is depicted in Fig. 1.

Calcined PZT powder of the composition $Pb(Zr_{0.52}Ti_{0.48})O_3$ prepared via conventional solid state reaction method was procured from CEL, India. Pure PZT powder was dispersed in unmodified and calcium modified PZT sols. Final slurries were prepared from powder loading level of 1.5 g:1 ml sol because this ratio resulted into the best quality films in terms of thickness and adhesion. The films obtained from powder loading level of 1 g:1 ml resulted into smaller film thickness of each layer and required more number of slurry layer deposition to get the desired film thickness. However, the powder loading level of 2.5 g:1 ml resulted into the films with poor adhesion to the surface of the substrate. Various dispersants were tried to make the slurries homogeneous but ESL 400 supplied by Electro Science Laboratories worked the best and hence was finally used.

2.2. Substrate cleaning

The substrate cleaning procedure used prior to film deposition greatly affects the adhesion of PZT films. The platinized silicon substrates ($Pt(1\,1\,1)/Ti/SiO_2/Si$) used in the present work were therefore methodically cleaned using following steps:

- Washed with soap solution using DI water.
- Completely immersed in trichloroethylene (works as degreaser) and ultrasonicated for 15 min.
- Ultrasonication in high purity isopropanol (IPA) for further 15 min.

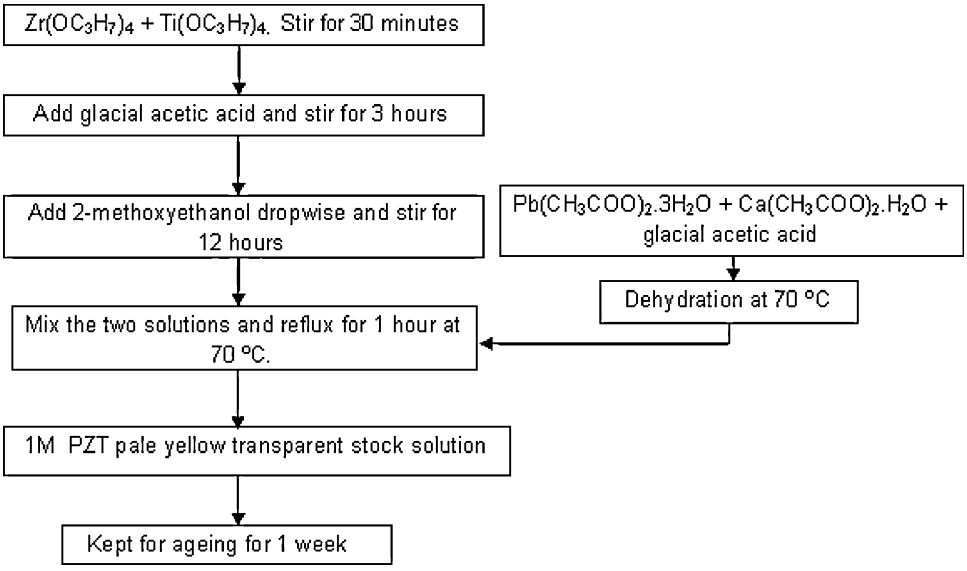

Fig. 1. Sol preparation process used in the present work.

- Dried and kept in clean room conditions prior to film deposition.

2.3. Film deposition

The resulting slurry and corresponding sol of each composition were alternatively deposited on platinized silicon substrates using spin coating technique at 3000 rpm for 1 min (for slurry) and 30 s (for dilute sol). The deposited films were dried at 150 °C for 15 min followed by pyrolysis at 350 °C for 15 min after each layer deposition. The basic idea of depositing the dilute sol after each layer of slurry deposition called infiltration process is to fill up the pores in order to obtain dense films. For that the sol is dropped onto the film after slurry deposition and pyrolysis, kept on spin coating unit with vacuum pump 'ON' for about a minute prior to spinning. This helps the sol to go deeper into the pores and the excess sol will go away by spinning process resulting in a uniform layer of sol. This process of depositing slurry and dilute sol alternatively, followed by drying and pyrolysis after deposition of each layer is continued up to 14 layers. The flow chart in Fig. 2 describes the process of making composite films. The annealed films with sol–gel matrix having 0, 6 and 10 mol% calcium content respectively were named as COMP0, COMP6 and COMP10. Higher temperature annealing of the films deposited on platinized silicon substrate is not recommended as it is well reported that above 750 °C, diffusion of silicon in PZT starts which deteriorates the properties of the final film.

3. Characterization

X-ray diffraction (XRD) (Philips, PW 1830 generator) technique has been utilized to examine the phase structure evolution of PZT thick films using Cu Kα radiation at room temperature. In order to analyze the adhesion strength of the film, AFM scratch test was performed using Veeco di CP II atomic force microscope in contact mode. The surface morphology and film thickness were observed by scanning electron microscopy (ZEISS, Model – MA15 and FEI Quanta 200F). For electrical measurements, gold electrodes with diameter of 1.5 and 2.5 mm were deposited on the top of the films through a mask using sputter coater (Desk II TSC Cold Sputter/Etch Unit). The dielectric constant (ε') and dissipation factor ($\tan\delta$) at room temperature with frequency and temperature dependence of dielectric constant were measured using Precision Impedence Analyzer (Wayne Kerr-6500B Series). While studying temperature dependence of dielectric constant, the measurement frequencies were chosen to be 100 Hz, 1 kHz, 5 kHz, 10 kHz, 50 kHz, 100 kHz, 500 kHz and 1 MHz. The polarization–electric field (P–E) behavior at room temperature was characterized by Automatic PE Loop Tracer supplied by Marine India Pvt. Ltd., New Delhi. The system

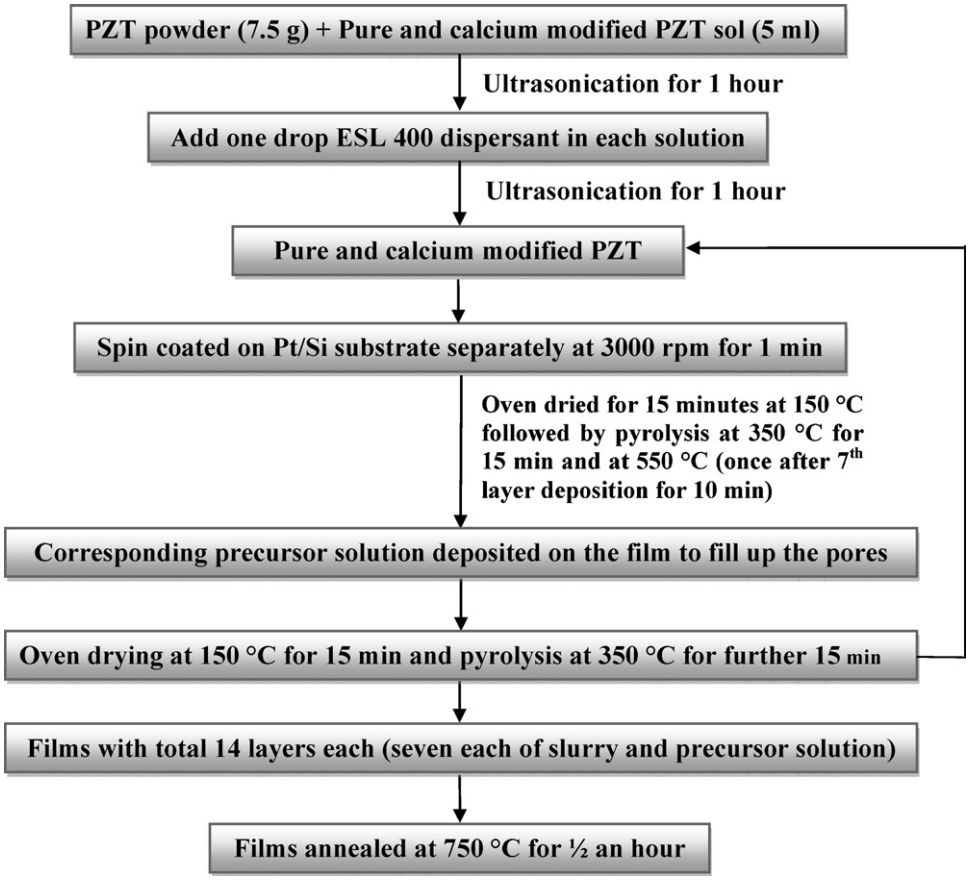

Fig. 2. Flow chart representation of composite sol–gel process used in the present work.

consists of a PC, Software, programmable voltage source (up to 5 kV) and probe type sample holder. The measurement is based on modified Sawyer Tower circuit, operating at 50 Hz.

4. Results and discussion

4.1. Testing the level of bonding between PZT thick film and the substrate (testing adhesion)

Generally, following two tests are employed to check the adhesion of the film with the substrate [19]:

- Scratch test – This test involves the use of metal blade to scratch the surface of a film in order to assess the adhesion between the film and the substrate. The films which are more easily removed have poor adhesion with the substrate surface.
- Tape test – This test involves sticking a strip of adhesive tape over the surface of a film and then peeling back the tape. The amount of material removed by the tape gives an indication of how well the film is adhered to the surface of the substrate. In fact, if any of the deposited film is removed by the tape, it is considered to have failed the test.

We used the scratch test to see the adhesion of the films on platinized silicon substrate. The films were not easily scratched and did not fall off when tapped on table. We also dipped a small annealed sample of a film in dilute hydrofluoric acid (HF) and it took a lot of time to be removed from the substrate which further confirmed very good adhesion of the film with the surface of the substrate.

Additionally, we tried to analyze the adhesion strength of the film through AFM scratch test using atomic force microscope in contact mode. We followed following steps:

Step 1: A 10 μm × 10 μm area was scanned at 500 nN. An area of 5 μm × 5 μm was chosen at 45° as shown by shaded area in Fig. 3(a) for application of higher load values.
Step 2: Applied 1500 nN load on shaded area.
Step 3: Followed by scanning the whole 10 μm × 10 μm area at 500 nN load value to see if any groove is created as a result of material removal/material pile up on sides of the shaded area.
Step 4: Step 3 was repeated after applying 2800 nN and 5000 nN (the maximum we could apply using the set up) loads on shaded area.

The topographic images of 10 μm × 10 μm scanned area after the application of different loads are shown in Fig. 3(b)–(e). No groove created because of application of the load is visible even after the application of 5000 nN load. On careful observation, particles are seen to be intact in their initial positions.

4.2. Microstructure and crystallinity

4.2.1. SEM analysis

Fig. 4(a) depicts surface morphology of one of the initial composite film prepared on platinized silicon substrate without using the infiltration process. The film is seen to be highly porous and it was impossible to make any electrical measurements on the film. Fig. 4(b) shows surface morphology of one of the composite films prepared on platinized silicon substrate using the infiltration process as described above in the present work. Fig. 4(c)–(e) shows the cross section of COMP0, COMP6 and COMP10 films respectively. Since surface morphology of all the films prepared in the present work using infilteration process was same, therefore only one micrograph has been shown. It can be seen from the cross section of the films that the films are of uniform thickness and the thickness measures approximately 31, 26 and 30 μm respectively for COMP0, COMP6 and COMP10 films. The platinum surface of the substrate has been marked in the figures. The surface morphology suggests that the thick films are crack free and homogeneous and consist of two types of grains. One has larger size (∼2 μm) and another one is granular having size in nanometer range. The former is from the powder particles loaded in the slurry while the latter one might have crystallized from xerogel solution. Thus, a composite structure is formed where larger grains are surrounded by the smaller grains. This kind of microstructure is a compromise result of microstructure and the overall dielectric/ferroelectric properties, and thus, will meet the requirement of both mechanical and electrical properties [20].

4.2.2. XRD analysis

X-ray diffraction patterns of PZT composite films deposited on platinized silicon substrate and annealed at 750 °C for half an hour show single phase perovskite structure as shown in Fig. 5. The peaks have been indexed as per the monoclinic structure. It can be also be seen from the XRD pattern that neither the pyrochlore phase nor a peak of (1 1 1) related to Pt were present. The absence of Pt(1 1 1) peak suggests that the films are thick and dense.

4.3. Dielectric properties

4.3.1. Frequency dependence of room temperature dielectric constant

The thick PZT films can be modeled as a 0–3 composite material, where the sol gel matrix is fully connected in three directions and the ceramic particles are not connected in any direction [14]. If the particles are uniformly dispersed in the sol gel matrix then the resulting dielectric constant is given by:

$$\varepsilon' = \varepsilon_2 \left[1 + \frac{3V_1(\varepsilon_1 - e_2)}{\varepsilon_1 + 2\varepsilon_2\text{-}V_1(\varepsilon_1\text{-}\varepsilon_2)} \right] \quad (1)$$

where ε_1 is the dielectric constant of the PZT powder, ε_2 is the dielectric constant of the sol gel matrix, and V_1 is the volume fraction of the ceramic powder. Eq. (1) is however valid only for the values of. $V_1 < 0.1$ at higher concentration, the dispersed phase starts to form continuous structures throughout the bulk that have non-zero connectivity. In that case, it becomes necessary to treat the composite as having phases connected in both series and parallel. When the material consists of two

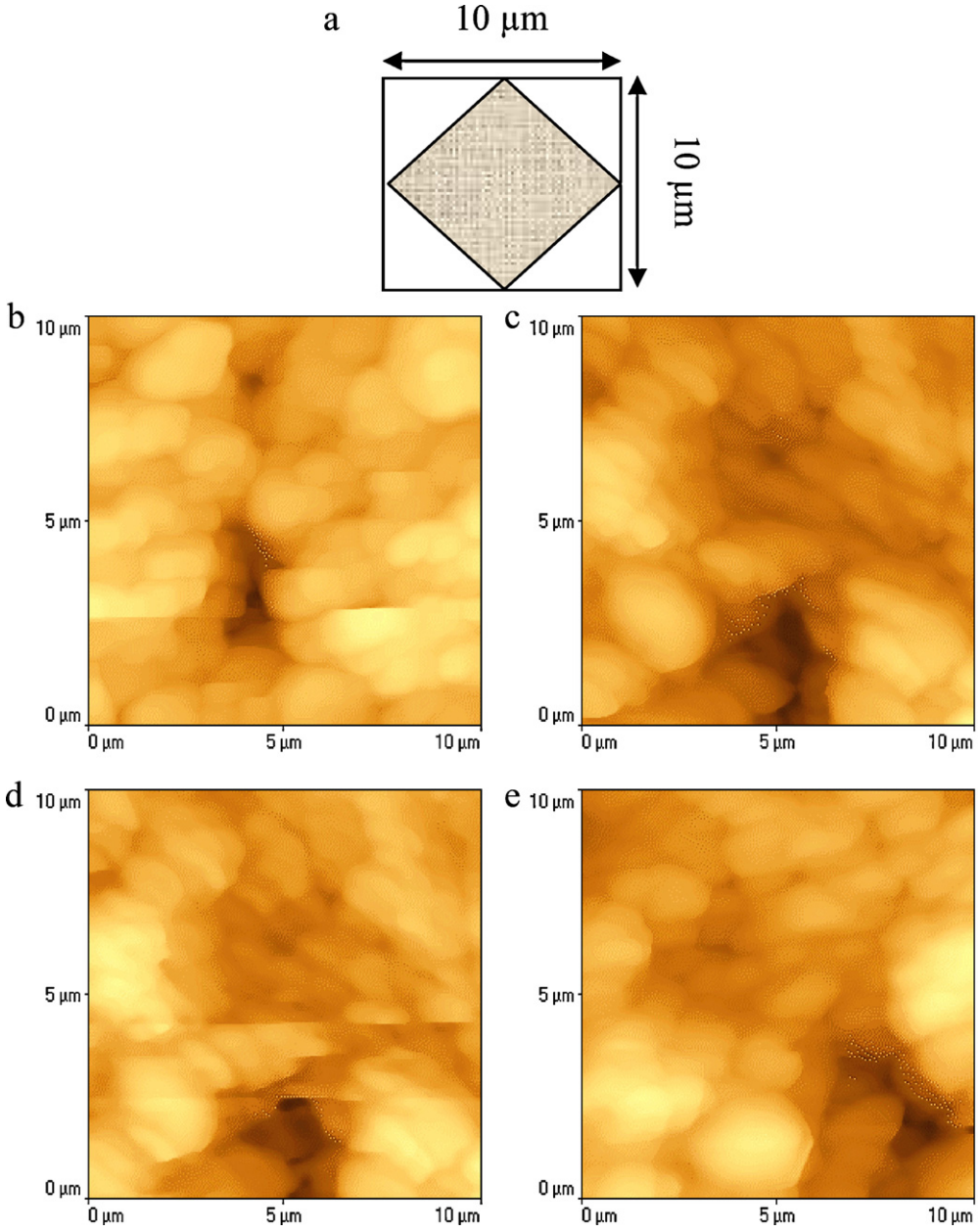

Fig. 3. (a) Shaded area (5 μm × 5 μm) chosen inside 10 μm × 10 μm scan area for application of different loads. (b)–(e) Topographic images with 10 μm × 10 μm area at 500 nN when load applied on the shaded area (5 μm × 5 μm) are 500 nN, 1500 nN, 2800 nN, 5000 nN respectively.

phases connected in parallel, the dielectric constant is given by:

$$\varepsilon' = V_1\varepsilon_1 + V_2 \cdot \varepsilon_2$$

where V_2 represents the volume fraction of sol–gel matrix. When the phases are connected in series, the dielectric constant is given by:

$$\frac{1}{\varepsilon'} = \frac{V_1}{\varepsilon_1} + \frac{V_2}{\varepsilon_2}$$

where $V_1 + V_2 = 1$. These cases represent the upper and lower bound of the dielectric constant.

However, there is more probability of a situation where the material exist in a combination of series and parallel phases as proposed in the cube model given by Pauer [21]. The dielectric constant in that case is given by:

$$\varepsilon' = [\frac{\varepsilon_1 + \varepsilon_2}{\{\varepsilon_2 - \varepsilon_1\} \cdot V_1^{-1/3} + \varepsilon_2 \cdot V_1^{-2/3})} + \varepsilon_2(1 - V_1^{-2/3}) \quad (2)$$

Frequency dependence of dielectric constant and dielectric loss at room temperature for the thick unpoled films are shown in Fig. 6. The values of room temperature dielectric constant (ε') and loss (tan δ) of the films COMP0, COMP6 and COMP10 on platinized silicon substrate at 10 kHz are presented in Table

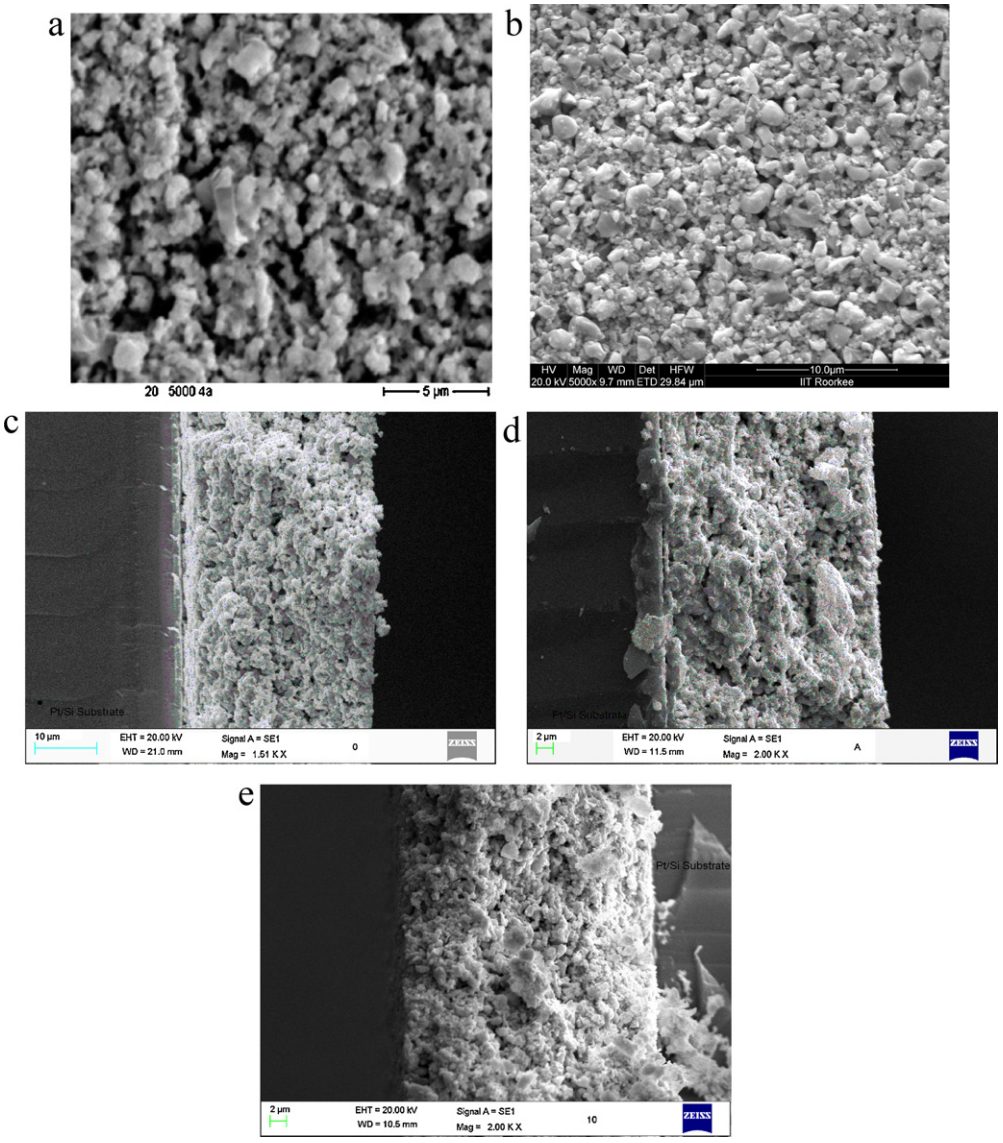

Fig. 4. (a) Surface morphology of initial composite films deposited without infiltration process on Pt/Si substrate and annealed at 750 °C; (b) surface morphology of composite films deposited using infiltration process on Pt/Si substrate and annealed at 750 °C characterized in the present work; (c)–(e) SEM micrographs of cross section of COMP0, COMP6, COMP10, respectively.

1. The value of dielectric constant follows increasing trend with increasing calcium content in the studied composition range.

4.3.2. *Temperature dependence of dielectric constant and loss*

The temperature dependence of the dielectric constant of the film is plotted as a function of frequency in Fig. 7. At higher temperatures, a peak in the dielectric constant is observed corresponding to the material passing through a phase transformation at the Curie temperature. However, the transition is gradual compared to sharp peak generally observed for bulk PZT. The dielectric constant at the Curie point is about twice its value at room temperature, in comparison to bulk ceramics which show an order of magnitude increase in permittivity at T_C. The broad nature of the peak can be attributed to various factors including film defects, slurry homogeneity, uniformity of film thickness, the presence of interfacial layers in the bottom electrode/film and film/top electrode interfaces and variation in the grain size of the composite films [11]. It is important to mention that though the magnitudes of the dielectric constant are different for the three samples, the value of transition temperature is same, i.e., 351 °C for the three samples. This suggests that the dielectric constant values are influenced by both phases but the transition temperature may be due to the powder added to the sol gel matrix because in the samples powder composition and its

Table 1
Room temperature dielectric constant and dielectric loss of composite films.

Sample Name	ε' (10 kHz)	tan δ (10 kHz)
COMP0	222.54	0.0337
COMP6	460.78	0.0236
COMP10	547.61	0.0344

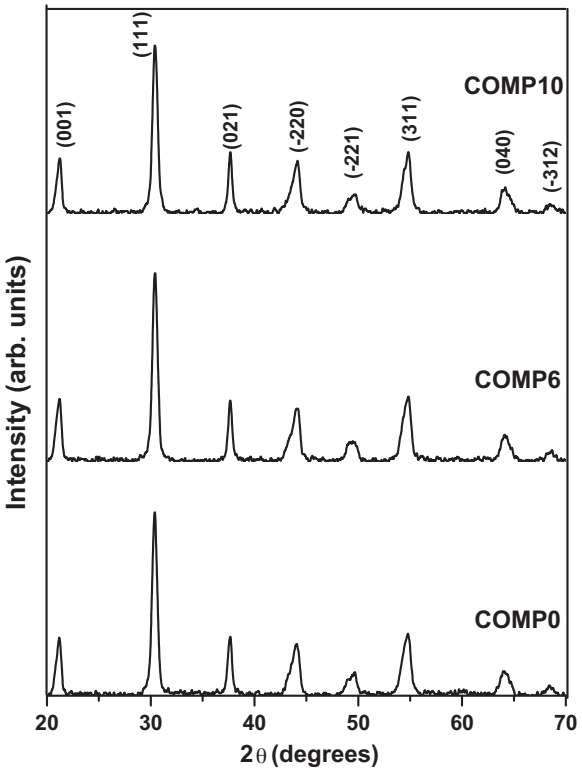

Fig. 5. XRD patterns of composite films.

amount were same and the sol gel matrix composition was different. Though, a detailed study is required to confirm whether it is actually because of the powder property or due to the phase which is present in greater volume fraction or is due to larger grained particles. In order to confirm whether it is due to the property of the powder, different types of powders with different T_C values may be used. Whether it is because of the phase that is present in larger amount may be confirmed by making T_C measurements on samples with different volume fraction of the powder. The effect of grain size can be studied by making the films via nano composite route.

Table 2
Polarization and coercive field values for the composite films at different values of applied electric field.

E_{max} (kV/cm)	Parameters	COMP0	COMP6	COMP10
120	P_r (μC/cm^2)	7.30	–	4.85
	P_s (μC/cm^2)	13.55	–	9.30
	E_c (kV/cm)	34.45	–	34.30
130	P_r (μC/cm^2)	–	6.87	5.51
	P_s (μC/cm^2)	–	12.98	10.26
	E_c (kV/cm)	–	36.92	36.90
150	P_r (μC/cm^2)	–	9.41	7.00
	P_s (μC/cm^2)	–	16.2	12.30
	E_c (kV/cm)	–	41.14	41.00
175	P_r (μC/cm^2)	–	11.76	8.00
	P_s (μC/cm^2)	–	18.86	13.32
	E_c (kV/cm)	–	50.94	50.00
200	P_r (μC/cm^2)	–	14.29	10.86
	P_s (μC/cm^2)	–	21.30	16.43
	E_c (kV/cm)	–	67.20	67.19

4.4. Ferroelectric properties

The polarization–electric field (PE) hysteresis curves for the films with the applied alternating field of strength ~150 kV/cm are shown in Fig. 8. As is evident from the figure all the films exhibit well saturated loops confirming evidence of ferroelectricity. In fact, the strength of applied alternating electric field was varied between 100 and 250 kV/cm and the PE loops as a function of driving electric field strength are shown in the inset of Fig. 8. The values of remanent polarization (P_r) and saturation polarization (P_s) as summarized in Table 2 for a given sample increase with increasing strength of applied electric field. It can also be seen from the values of polarization and coercive field that the increasing calcium content in the sol–gel matrix has a greater impact on P_r and P_s values while E_c is almost same for all the films for a given strength of applied field. In the studied composition range, P_r and P_s values show a decreasing trend for a given driving field with increasing calcium content in the sol–gel matrix used in making thick

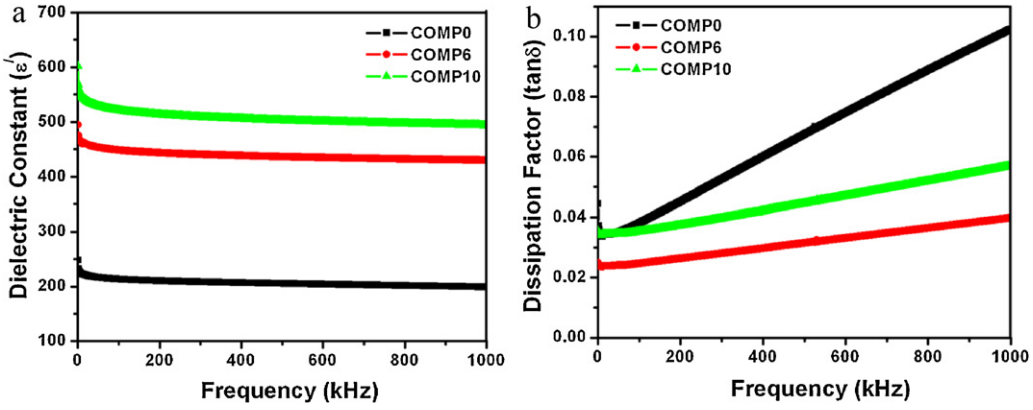

Fig. 6. (a) Frequency dependence of room temperature dielectric constant and (b) frequency dependence of room temperature dielectric loss of composite films.

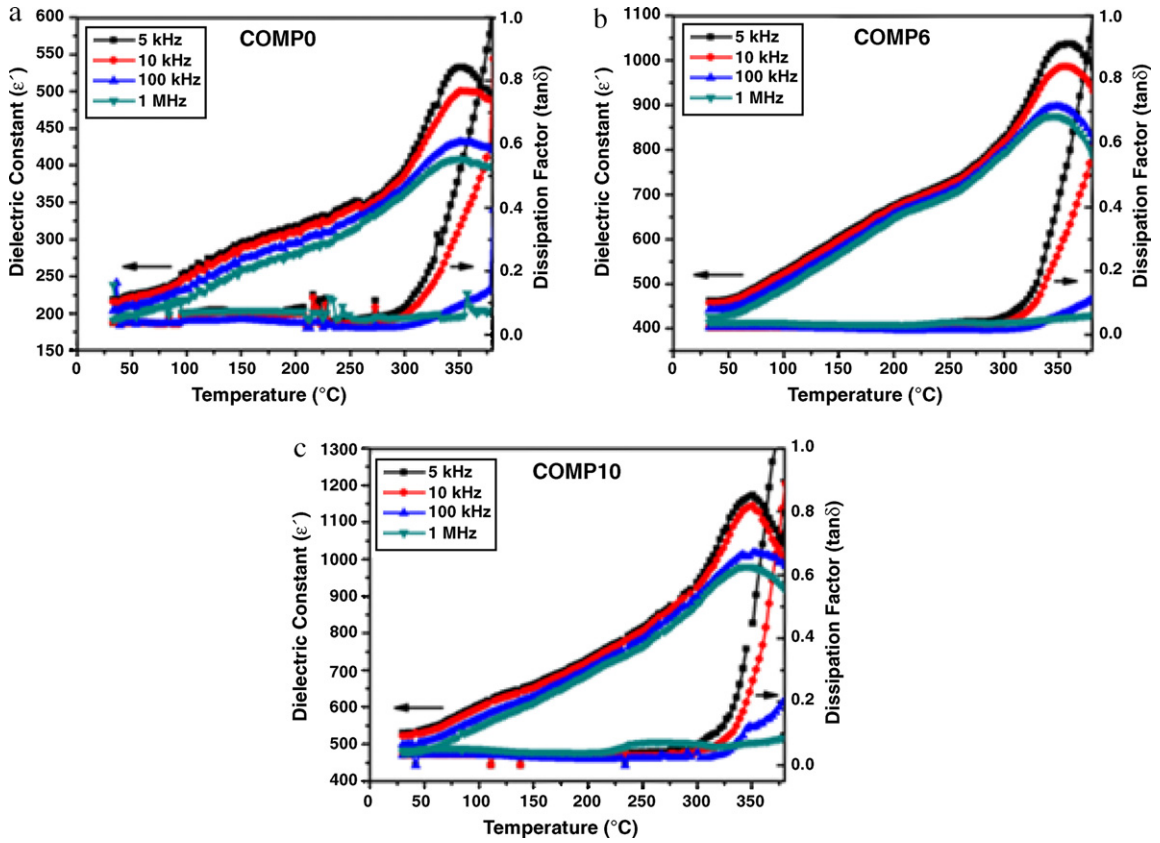

Fig. 7. Temperature dependence of dielectric constant and loss for composite films.

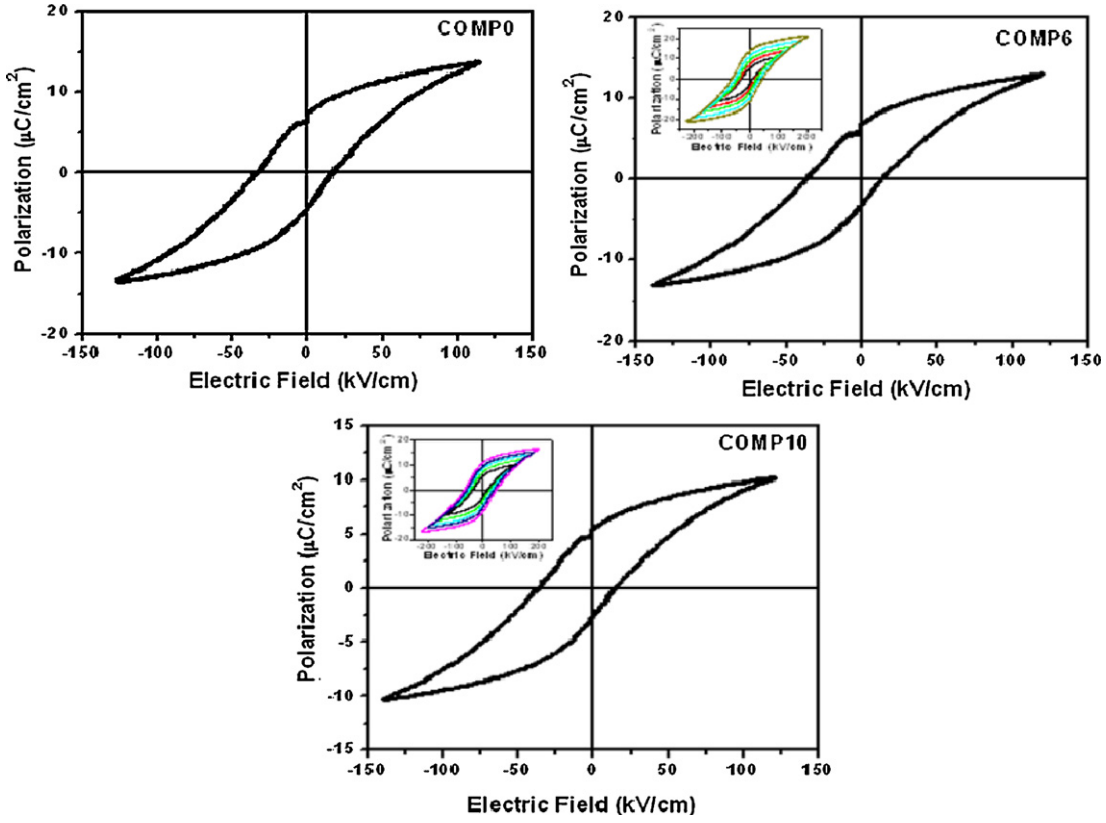

Fig. 8. PE–hysteresis loops for composite films (inset figures showing PE loops at various driving electric field strengths).

films. We may infer that the value of polarization may be governed by the properties of composite slurry. On the other hand, coercive field which is seen to be almost same for all the three compositions for a given driving field is dependent on the properties of the powder because the same powder with same powder to sol ratio was added to make corresponding composite slurries.

5. Conclusions

Crack free calcium modified PZT composite films of thickness in the range from 26 to 31 μm have been prepared successfully on Pt/Si substrate using modified sol–gel process. Infiltration process has also been used which results in dense microstructure of the films. Dielectric studies performed on the films reveal that the room temperature dielectric constant follows the similar trend as that of sol–gel derived calcium modified bulk samples with overall dielectric constant being smaller than the corresponding bulk ceramics. An interesting feature that has been noticed is that all three samples, in spite of the different composition of the sol used, exhibit same T_C value. Ferroelectric loops of the films reveal that though P_r may be dependent on both powder and sol phases, E_c seems to be dependent on powder properties in the studied compositions. This investigation may be useful in fabricating composite films with desired properties for specific applications.

Acknowledgments

One of the authors (Anupama Sachdeva) is grateful to V.P.S. Tyagi, Vandna Luthra and N.C. Mehra for their support and guidance in experimental work. Thanks are also due to Prikshit Gautam for useful discussions.

References

[1] P. Muralt, M. Kohli, T. Maeder, A. Kholkin, K.G. Brooks, N. Setter, R. Luthier, Fabrication and characterization of PZT thin-film vibrators for micromotors, Sens. Actuators A 48 (1995) 157–165.
[2] P. Muralt, PZT thin films for microsensors and actuators: where do we stand? IEEE Trans. Ultrason. Ferroelect. Freq. Control. 47 (2000) 903–991.
[3] A. Schroth, C. Lee, S. Matsumoto, M. Tanaka, R. Maeda, Application of sol–gel deposited thin PZT film for actuation of 1D and 2D scanners, Sens. Actuators A 73 (1999) 144–152.
[4] C.J. Pavlin, M.D. Sherar, F.S. Foster, Subsurface ultrasound microscopic imaging of the intact eye, Ophthalmology 97 (1990) 244–250.
[5] G. Yi, M. Sayer, Bull. Ceram, Sol–gel processing of complex oxide films, Ceram. Bull. 70 (7) (1991) 1173–1179.
[6] R. Zimmermann-Chopin, S. Auer, Spray drying of sol–gel precursors for the manufacturing of PZT powders, J. Sol–Gel Sci. Technol. 3 (1994) 101–107.
[7] M. Sayer, G. Yi, M. Sedlar, Comparative sol gel processing of PZT thin films, Integr. Ferroelectr. 7 (1995) 1–4.
[8] K. Miyazawa, K. Ito, R. Maeda, Structure, Electrical properties of sol–gel processing, Ceram. Int. 26 (2000) 501–506.
[9] G. Yi, Z. Wu, M. Sayer, Preparation of $Pb(Zr,Ti)O_3$ thin films by sol gel processing: electrical optical and electro-optic properties, J. Appl. Phys. 64 (1988) 2717–2724.
[10] Y.C. Hsu, C.C. Wu, C.C. Lee, G.Z. Cao, I.Y. Shen, Demonstration and characterization of PZT thin-film sensors and actuators for meso- and micro-structures, Sens. Actuators A 116 (2004) 369–377.
[11] H.D. Chen, K.R. Udayakumar, L.E. Cross, J.J. Bernstein, L.C. Niles, Dielectric, ferroelectric and piezoelectric properties of lead zirconate titanate thick films on silicon substrate, J. Appl. Phys. 77 (1995) 3349–3353.
[12] E.S. Thiele, N. Setter, Processing and properties of screen-printed lead zirconate titante piezoelectric thick films on electroded silicon, J. Am. Ceram. Soc. 84 (2001) 2863–2868.
[13] R. Mass, M. Koch, N.R. Harris, N.M. White, A.G.R. Evans, Thick film printing of PZT onto silicon, Mater. Lett. 31 (1997) 109–112.
[14] D.A. Barrow, T.E. Petroff, R.P. Tandon, M. Sayer, Characterization of thick lead zirconate titanate films fabricated using a new sol gel based process, J. Appl. Phys. 81 (1997) 876–881.
[15] M.K. Cheung, K.W. Kwok, H.L.W. Chan, C.L. Choy, Dielectric and pyroelectric properties of lead zirconate titanate composite films, Integr. Ferroelectr. 54 (2003) 713–719.
[16] Z. Wang, W. Zhu, C. Zhao, O.K. Tan, Dense PZT thick films derived from sol–gel based nanocomposite process, Mater. Sci. Eng. B 99 (2003) 56–62.
[17] M.K. Cheung, K.W. Kwok, H.L.W. Chan, C.L. Choy, Preparation, Characterization of ceramic/ceramic composite films, Jpn. J. Appl. Phys. 44 (2005) 1847–1851.
[18] Q.Q. Zhang, F.T. Djuth, Q.F. Zhou, C.H. Hu, J.H. Cha, K.K. Shung, High frequency broadband PZT thick film ultrasonic transducers for medical imaging applications, Ultrasonics 44 (2006) e711–e715.
[19] D.P.J. Cotton, P.H. Chappell, A. Cranny, N.M. White, A new binderless thick-film piezoelectric paste, J. Mater. Sci.: Mater. Electron. 18 (2007) 1037–1044.
[20] C. Zhao, Z. Whang, W. Zhu, O. Tan, H. Hng, Microstructure and properties of PZT53/47 thick films derived from sols with submicron-sized PZT particle, Ceram. Int. 30 (2004) 1925–1927.
[21] L.A. Pauer, Flexible piezoelectric material, IEEE Int. Conv. Rec. (1973) 1–5.